Since January 2020 Elsevier has created a COVID-19 resource centre with free information in English and Mandarin on the novel coronavirus COVID-19. The COVID-19 resource centre is hosted on Elsevier Connect, the company's public news and information website.

Journal of Hazardous Materials 423 (2022) 127144

Contents lists available at ScienceDirect

Journal of Hazardous Materials

journal homepage: www.elsevier.com/locate/jhazmat

Repercussions of clinical waste co-incineration in municipal solid waste incinerator during COVID-19 pandemic

Dong-Ying Lan [a], Hua Zhang [a,b,c,*], Ting-Wei Wu [a], Fan Lü [a,b,c], Li-Ming Shao [a,b,c], Pin-Jing He [a,b,c]

[a] Institute of Waste Treatment & Reclamation, College of Environmental Science and Engineering, Tongji University, Shanghai 200092, China
[b] Shanghai Institute of Pollution Control and Ecological Security, Shanghai 200092, China
[c] Shanghai Engineering Research Center of Multi-source Solid Wastes Co-processing and Energy Utilization, Shanghai 200092, China

ARTICLE INFO

Editor: Zaher Hashisho

Keywords:
Coronavirus disease 2019
Feedstock properties
Acid gas emission
Distribution of major elements
Heavy metals volatilization

ABSTRACT

During coronavirus disease 2019 pandemic, the exponential increase in clinical waste (CW) generation has caused immense burden to CW treatment facilities. Co-incineration of CW in municipal solid waste incinerator (MSWI) is an emergency treatment method. A material flow model was developed to estimate the change in feedstock characteristics and resulting acid gas emission under different CW co-incineration ratios. The ash contents and lower heating values of the feedstocks, as well as HCl concentrations in flue gas showed an upward trend. Subsequently, 72 incineration residue samples were collected from a MSWI performing co-incineration (CW ratio <10 wt%) in Wuhan city, China, followed by 20 incineration residues samples from waste that were not co-incineration. The results showed that the contents of major elements and non-volatile heavy metals in the air pollution control residues increased during co-incineration but were within the reported ranges, whereas those in the bottom ashes revealed no significant changes. The impact of CW co-incineration at a ratio <10 wt% on the distribution of elements in the incineration residues was not significant. However, increase in alkali metals and HCl in flue gas may cause potential boiler corrosion. These results provide valuable insights into pollution control in MSWI during pandemic.

1. Introduction

Coronavirus disease 2019 (COVID-19) is an acute respiratory disease that emerged in late 2019, resulting in a pandemic (Zhou and Shi, 2021). According to the World Health Organization report, COVID-19 has affected 223 countries with around 174 million confirmed infected cases and 3.7 million deaths until June 11, 2021 (World Health Organization, 2020). During such an outbreak, a substantial amount of clinical waste (CW) has been generated (Prata et al., 2020). Due to the vast consumption of clinical resources and personal protective equipment to mitigate the pandemic, the CW generation rates of confirmed and suspected cases have been predicted to be 3.2 and 1.8 kg/(bed × day), respectively, which are 4- and 2-fold higher than those of patients with other diseases (0.8 kg/(bed × day)) (Wang et al., 2021). For example, the daily generation of CW in Wuhan city in March 2020 was 5-fold higher than that in March 2019 (You et al., 2020). In addition, domestic waste produced by emergency medical centers and quarantine points are often processed as CW owing to their potential infection hazard (Yang et al., 2021). A previous investigation indicated the strong stability of coronavirus on the surfaces of plastics and stainless steel for up to 72 h, and on cardboard surfaces for up to 48 h (van Doremalen et al., 2020). Therefore, environment-friendly treatment and disposal of CW is essential to protect human health during COVID-19 outbreak.

The sharp increase in CW generation threatens to overwhelm local treatment capacity. To address the overflow of CW, co-incineration in municipal solid waste incinerator (MSWI) is an emergency option and a feasible choice because grate incinerator with high heat transfer rate and operating temperature (> 850 ℃) guarantees reliable destruction of pathogens (Neuwahl et al., 2010). At the same time, the decline in the generation of municipal solid waste (MSW) during the pandemic provides sufficient CW treatment capacity.

Nevertheless, information about the risks arising from co-incineration, such as production and emission of secondary pollutants is limited. The nature and composition of CW significantly vary from those of MSW, and specific CW often contains materials with high lower heating values (LHV) and ash contents (e.g., metals) (Neuwahl et al.,

* Corresponding author at: Institute of Waste Treatment and Reclamation, Tongji University, Shanghai 200092, China.
E-mail address: zhanghua_tj@tongji.edu.cn (H. Zhang).

https://doi.org/10.1016/j.jhazmat.2021.127144
Received 12 June 2021; Received in revised form 24 August 2021; Accepted 2 September 2021
Available online 15 September 2021

2010; Patrício Silva et al., 2021). Meanwhile, the use of plastic products, such as personal protective equipment (gloves, masks, and protective gown) (Jędruchniewicz et al., 2021), which are essential to reduce the transmission of this highly contagious virus, has raised attention owing to the resulting increase in the proportion of plastic waste in CW (Prata et al., 2020; Patrício Silva et al., 2021; Shammi et al., 2021). Thus, inappropriate operation of co-incineration may cause incomplete combustion (Neuwahl et al., 2010), enhancing the emission of aromatic compounds and acid gases as well as generating residue of unacceptable quality.

The main aim of this study was to quantitatively evaluate the potential impacts of CW co-incineration in MSWI. First, the various compositions and properties of CW and MSW, as well as the co-incineration ratios of CW treated in MSWI were examined. The fluctuation of LHV and ash contents of the co-incinerated waste feedstock (CIWF) and source strengths of HCl and SO_2 in the flue gas were explored via simulated calculation based on proximate and ultimate analysis data of CW and MSW available in scientific literature. Then, the incineration residues from a MSWI plant in Wuhan city during and after COVID-19 outbreak, i.e., with and without co-incineration, were collected and characterized. The policies and experience of CW management in Wuhan city have been summarized in previous studies (Yang et al., 2021; Yu et al., 2020; Wang et al., 2020). Before the COVID-19 outbreak, CW had been predominantly treated in centralized disinfection facilities and CW incinerators which can handle steady-state conditions (Yang et al., 2021; Purnomo et al., 2021). However, during COVID-19 outbreak, co-incineration had to be performed to manage the dramatic increase in CW. Therefore, the contents of major elements and heavy metals in the incineration residues were determined and compared. Furthermore, the effects of CW co-incineration on the fate of major elements and heavy metals as well as potential boiler corrosion were examined by statistical analysis. The findings of this study provide further insights into the risk assessment of CW treated in MSWI, thereby serving as a guide to safe application.

2. Materials and methods

2.1. Prediction calculation using material flow model

2.1.1. Composition data of MSW and CW

The physical and elemental compositions of MSW and CW were obtained from the literature and filtered in accordance with the following principles: (i) physical compositions and proximate analysis data were based on wet basis and (ii) ultimate analysis and higher heating values data were based on dry basis.

In total, 62 and 31 sets of physical compositions of MSW (Table S1) and CW (Table S2) were obtained, respectively, with $62 \times 31 = 1922$ permutations of co-incineration mode between MSW and CW with each co-incineration ratio. Tables S3 and S4 show the proximate and ultimate analysis data and higher heating value data of typical fractions for MSW and CW, respectively, of which, the mean values were used for prediction calculations.

2.1.2. Calculation methods using material flow model

For assessing the effects of CW co-incineration in MSW incinerator, the LHV and ash contents of CIWF and the concentrations of HCl and SO_2 in flue gas from co-incineration were predicted as shown in Eqs. (1)–(13).

First, the ultimate analysis results were transformed from dry basis to wet basis, and the elemental compositions of CIWF with different CW co-incineration ratios were calculated as follows:

$$E^{fx}_{wet} = E^{fx}_{dry} \times \left(1 - \frac{M^{f}_{wet}}{100}\right) \tag{1}$$

$$E^{x}_{wet} = \left(1 - \frac{R_i}{100}\right) \times \sum_{y}\left(\frac{MSW^{y}_{wet}}{100} \times E^{yx}_{wet}\right) + \frac{R_i}{100} \times \sum_{z}\left(\frac{CW^{z}_{wet}}{100} \times E^{zx}_{wet}\right) \tag{2}$$

where E^{fx}_{wet} and E^{fx}_{dry} are the contents of element x in organic component f on a wet basis and dry basis, respectively (%); M^{f}_{wet} is the moisture content of organic component f (%); x refers to C, H, O, N, S, Cl; f refers to the organic component y in MSW (food waste, wood waste, paper, textile, plastic, and rubber) or the organic component z in CW (plastic, paper, textile, tissue, and food waste); E^{x}_{wet} is the content of element x in CIWF on a wet basis (%); R_i is the ratio of CW co-incineration, i.e., 0%, 5%, 10%, 15%, and 20%; MSW^{y}_{wet} is the percentage of organic component y (food waste, wood waste, paper, textile, plastic, and rubber) in MSW (%); and CW^{z}_{wet} is the percentage of organic component z in CW (plastic, paper, textile, tissue, and food waste) (%). Glass, metals, and other incombustible substances (Lin et al., 2015) were treated as ash in CIWF.

Similar calculations were conducted for determining the moisture and ash contents, as well as LHV of CIWF based on the physical compositions of MSW and CW. LHV of CIWF were calculated based on the elemental compositions using Dulong formula (see Supporting Information (SI)).

Subsequently, the source strengths of acid gas in flue gas from CIWF incineration were deduced, as shown in Eqs. (3)–(12). Flue gas is mainly composed of N_2, CO_2, H_2O, O_2, SO_2, and HCl (Peng et al., 2016). The excess air ratio was set as 2.1, which is often used for full-scale incinerators.

$$V(A_0) = \frac{\left(\frac{E^{H}_{wet}}{4 \times 100} - \frac{E^{Cl}_{wet}}{35.5} + \frac{E^{C}_{wet}}{12 \times 100} + \frac{E^{S}_{wet}}{32 \times 100} - \frac{E^{O}_{wet}}{32 \times 100}\right) \times 22.4}{0.21} \tag{3}$$

$$V(CO_2) = \frac{E^{C}_{wet} \times 22.4}{12 \times 100} \tag{4}$$

$$V(SO_2) = \frac{E^{S}_{wet} \times 22.4}{32 \times 100} \times r \tag{5}$$

$$V(HCl) = \frac{E^{Cl}_{wet} \times 22.4}{35.5 \times 100} \tag{6}$$

$$V(H_2O) = \left(\frac{E^{H}_{wet}}{2 \times 100} - \frac{E^{Cl}_{wet}}{35.5} + \frac{M_{wet}}{18 \times 100}\right) \times 22.4 \tag{7}$$

$$V(O_2) = V(A_0) \times 1.1 \times 0.21 \tag{8}$$

$$V(N_2) = V(A_0) \times 2.1 \times 0.79 + \frac{E^{N}_{wet} \times 22.4}{28 \times 100} \tag{9}$$

$$V(G) = V(CO_2) + V(SO_2) + V(HCl) + V(H_2O) + V(O_2) + V(N_2) \tag{10}$$

$$M(SO_2) = \frac{E^{S}_{wet} \times 64}{32 \times 100} \times r \tag{11}$$

$$M(HCl) = \frac{E^{Cl}_{wet} \times 36.5}{35.5 \times 100} \tag{12}$$

$$C(j) = \frac{M(j)}{V(G)} \times 10^6 \tag{13}$$

where $V(A_0)$ is the theoretical air demand for incineration of 1 kg of CIWF (Nm^3/kg CIWF); $V(CO_2)$, $V(SO_2)$, $V(HCl)$, $V(H_2O)$, $V(O_2)$, and $V(N_2)$ are the normalized volume of CO_2, SO_2, HCl, H_2O, O_2, and N_2,

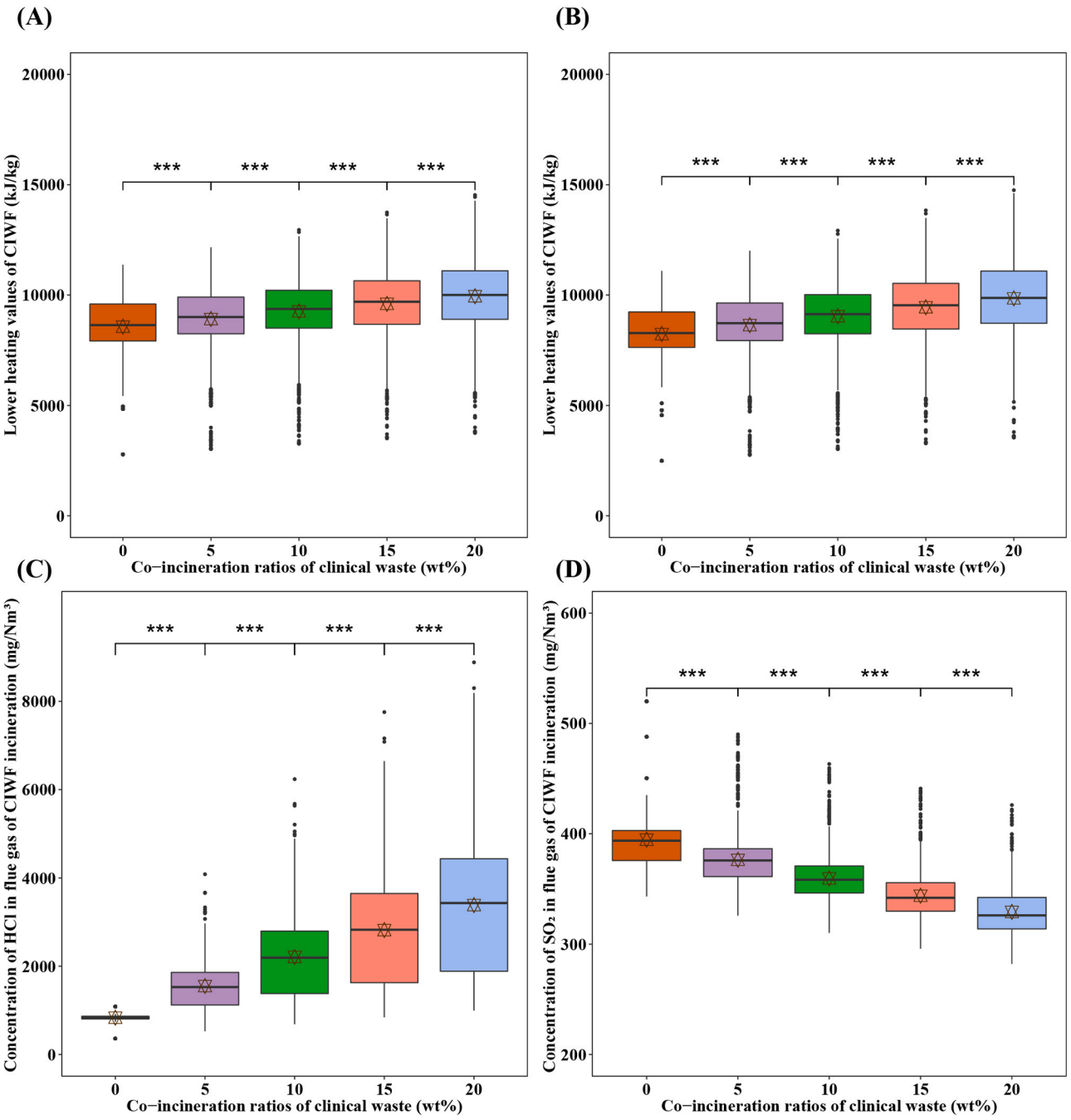

Fig. 1. Estimated results for the co-incinerated waste feedstock (CIWF) with different clinical waste (CW) co-incineration ratios in wet basis. Lower heating values (LHV) of CIWF based on Dulong formula (A); LHV of each component of municipal solid waste and CW from the literatures (B); concentration of HCl in flue gas (C); and concentration of SO_2 in flue gas (D). Median, 25th, and 75th percentiles are plotted as the horizontal solid lines of the boxes. The six-pointed stars represent mean values. The upper and lower whiskers extend to data no more than 1.5 times of the interquartile range from the upper and lower edge of the box, respectively. The black dots represent outliers. The results obtained with different CW co-incineration ratios were compared (*P* values were computed using Student's *t*-test, *** denotes $P < 0.001$, i.e., difference in mean value is statistically significant).

respectively, generated by incineration of 1 kg of CIWF (Nm^3/kg CIWF); $V(G)$ is the normalized volume of gas generated by incineration of 1 kg of CIWF (Nm^3/kg CIWF); E^{C}_{wet}, E^{H}_{wet}, E^{O}_{wet}, E^{S}_{wet}, E^{Cl}_{wet}, and E^{N}_{wet} are the contents of C, H, O, S, Cl, and N in CIWF on a wet basis, respectively (%); r is the transfer ratio of S from CIWF to gaseous sulfur compounds, considered as SO_2, along with flue gas, and is set to 0.35 according to previous studies (Belevi and Moench, 2000; Huang et al., 2018; Zhang et al., 2019); $M(SO_2)$ and M(HCl) are the amounts of SO_2 and HCl generated from incineration of 1 kg of CIWF, respectively (kg/kg CIWF); and $C(j)$ is the normalized concentration of j (HCl or SO_2) in the flue gas (mg/Nm^3). The entire Cl in the feedstock was considered to be discharged into flue gas as HCl.

2.1.3. *Uncertainty analysis*

The d-factor was adopted to quantify the uncertainty of the calculation results. In general, a higher d-factor for a parameter indicates that it has greater influence on the results (Ma et al., 2020; Talebizadeh and Moridnejad, 2011). All the physical composition values of plastic, paper, textile, and tissue in CW as parameters were assumed to fluctuate by ± 10%, and the changes in the predicted results were observed with CW

Table 1
Uncertainty analysis (d-factors) of the effects of clinical waste components on the estimated results.

Component	$LHV(\text{Dulong})_{wet}$	$LHV(\text{literature})_{wet}$	Ash	HCl	SO_2
plastic	0.13	0.13	0.00	0.14	-0.08
paper	0.02	0.03	0.00	-0.01	-0.02
textile	0.03	0.03	0.01	-0.01	-0.03
tissue	0.00	0.00	0.00	0.00	0.00

$LHV(\text{Dulong})_{wet}$: estimated lower heating values (LHV) based on Dulong formula; $LHV(\text{literature})_{wet}$: estimated LHV based on the LHV results of each component of MSW and CW from the literatures.

co-incineration ratio of 20%.

$$\overline{d_X} = \frac{1}{k} \times \sum_{m=1}^{k} (X_{2m} - X_{1m}) \tag{14}$$

$$d - factor = \frac{\overline{d_X}}{\sigma_X} \tag{15}$$

where $\overline{d_X}$ is the sum of the difference between the estimated result after parameter fluctuation X_{2m} and that before parameter fluctuation X_{1m}, σ_X is the standard deviation of the estimated results before fluctuation, and k is the number of data groups (co-incineration mode; $k = 1922$).

2.2. Experimental methods

During the COVID-19 pandemic between March and May 2020, co-incineration of CW was performed in a MSWI plant in Wuhan city. The co-incinerated CW included those from designated hospitals, shelter hospital, and isolation locations. The general information and material flow are summarized in Tables S5 and S6. To investigate the effect of CW co-incineration ratios on MSWI, 40 air pollution control (APC) residues and 32 bottom ash (BA) samples with different CW input amounts, named as CWG, were collected. For comparison, 10 APC residues and 10 BA samples from the same MSWI without CW co-incineration, named as NCWG, were also collected (June – July 2020). The specific co-incineration amounts of CW per day during sampling are tabulated in Table S6. It can be noted from the table that the co-incineration ratios of CW were < 10 wt% of the incinerated MSW. All the incineration residues samples were dried at 105 C for 24 h.

The relative contents of major elements in the incineration residues were determined by X-ray fluorescence spectrometer (XRF-1800, Shimadzu, Japan). The contents of heavy metals in the APC residues were measured by inductively coupled plasma optical emission spectroscopy (ICP-OES) (5100-OES, Agilent, USA) after acid digestion according to EPA Method 3050B (United States Environmental Protection Agency, 1996).

All the chemicals and reagents utilized in this study were purchased from Sinopharm Chemical Reagent Co., Ltd. (China), including concentrated HCl, HNO_3, HF, $HClO_4$, etc., and all the solutions employed for the experiments were prepared using Milli-Q water.

2.3. Multivariate data analysis

Descriptive statistics and correlation analysis were performed to evaluate the calculated and analytical data using Python (version 3.8.3) and R studio (version 4.0.2) software.

3. Results and discussion

3.1. Effect of CW co-incineration on CIWF properties and acid gas emissions

3.1.1. Predicted results

The estimated LHV and ash contents of CIWF under various CW co-incineration ratios (0%, 5%, 10%, 15%, and 20%) are summarized in Figs. 1A, B, and S1. $LHV(\text{Dulong})_{wet}$ and $LHV(\text{literature})_{wet}$ were 8691 ± 1563 kJ/kg (Fig. 1A) and 8233 ± 1558 kJ/kg (Fig. 1B), respectively, when the CW co-incineration ratio was 0%. Similar LHV results were obtained using two different methods, and the LHV of CIWF showed an upward trend with the increasing CW co-incineration ratio. Moreover, the ash contents of CIWF significantly increased from 11% ± 7–15% ± 6% as the CW co-incineration ratio was increased from 0% to 20% (Fig. S1), which was mainly caused by the inorganic components (glass and metals) in CW (Table S4).

The concentrations of HCl and SO_2 in flue gas under different CW co-incineration ratios are shown in Fig. 1C and D. The HCl concentrations were 825 ± 78, 1536 ± 438, 2190 ± 804, 2795 ± 1119, and 3359 ± 1392 mg/Nm^3 when the CW co-incineration ratios were 0%, 5%, 10%, 15%, and 20%, respectively (Fig. 1C), whereas the corresponding SO_2 concentrations were 395 ± 28, 376 ± 23, 359 ±21, 344 ± 21, and 329± 21 mg/Nm^3, respectively (Fig. 1D). Thus, a significant increase ($P < 0.001$) in HCl concentration and decline ($P < 0.001$) in SO_2 concentration were observed with the increase in CW amounts.

These results are in agreement with the reported actual concentrations of HCl and SO_2 in MSWI flue gas from boiler (about 500–2000 and 200–1000 mg/Nm^3, respectively) (Neuwahl et al., 2010; Zhang et al., 2019; Bai, 2009). It should be noted that the concentration of HCl reached or exceeded the maximum of this range in MSWI when the CW co-incineration ratio was >10%. These findings confirmed that the ratio of CW treated in MSWI should be limited.

3.1.2. Uncertainty analysis

The results of uncertainty analysis of the impact factors, contents of plastic, paper, textile, and tissue in CW are presented in Table 1. The variation in plastic proportion showed significant effects on the estimated $LHV(\text{Dulong})_{wet}$ and $LHV(\text{literature})_{wet}$ of CIWF, as well as the source strengths of HCl in flue gas, with d-factors of 0.13, 0.13, and 0.14, respectively. Paper and textile exhibited similar influences on the estimated results, whereas tissue proportion exerted minimum influence.

The use of plastic products has sharply increased for achieving protection from COVID-19 infection, which has resulted in subsequent massive generation of plastic waste (Klemeš et al., 2020; Zhou et al., 2021; Jung et al., 2021). Plastic waste with high organic carbon content, which is a statistically significant predictor of LHV (Komilis et al., 2012), can increase the average LHV of feedstock in co-incineration plants (Fig. 1A, Table 1), thus influencing the temperature of the furnace. Furthermore, the Cl content in PVC, one of the main compounds in plastic waste (e.g., syringes, vinyl gloves) (Klemeš et al., 2020; Sharma et al., 2020) can enhance HCl emission (Fig. 1C) and formation of chlorinated aromatic compounds (Vejerano et al., 2013). Therefore, the exhaust gas emissions from stack must be monitored when CW is co-incinerated in MSWI, and if an increasing trend is detected, then the operation parameters of the APC system should be adjusted to ensure compliance with the emission limits, especially the semi-dry scrubber for absorbing acid gas and activated carbon injection for removal of heavy metals and chlorinated aromatic compounds.

3.1.3. Limitation of prediction calculation

Prediction calculation using material flow model helps to investigate the influence of CW co-incineration on feedstock LHV and acid gas

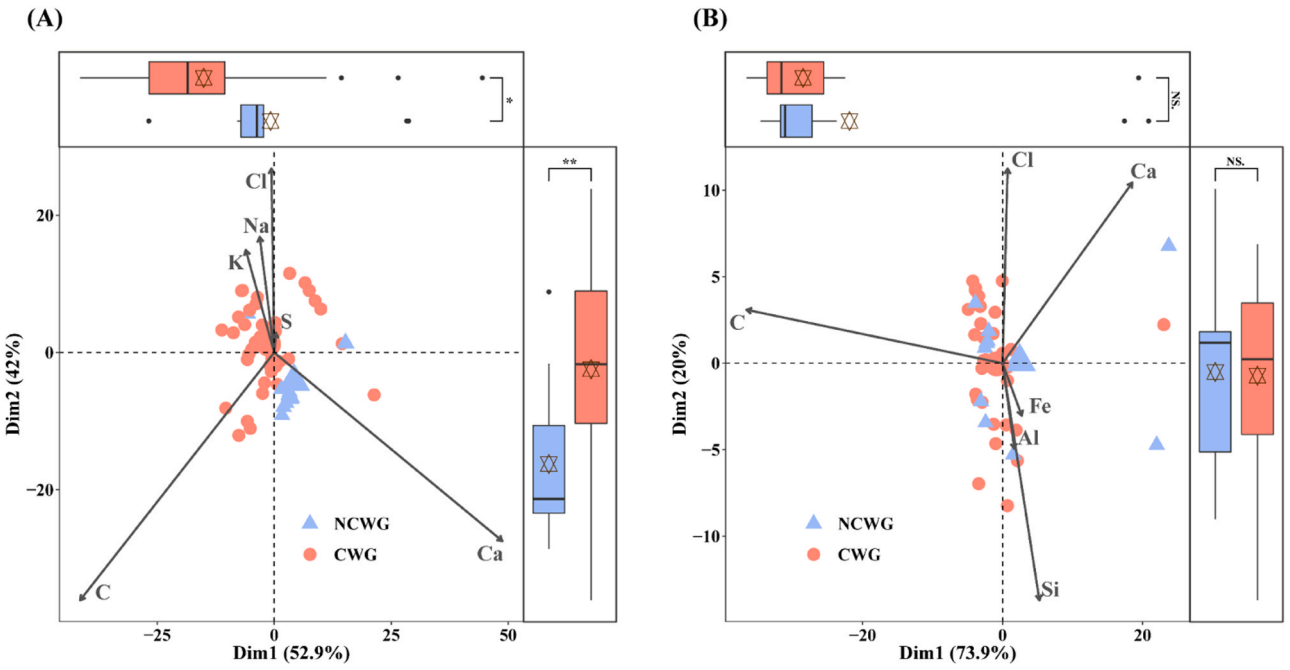

Fig. 2. Element-based principal component analysis of air pollution control residues (A) and bottom ash (B). NCWG and CWG denote incineration residue samples from incinerator without and with clinical waste input, respectively. Box plots show the overall distribution of Dim1 and Dim2 within NCWG and CWG (Student's *t*-test; NS represents $P > 0.05$, * denotes $0.01 < P < 0.05$, ** signifies $0.001 < P < 0.01$, * and ** indicate statistically significant difference).

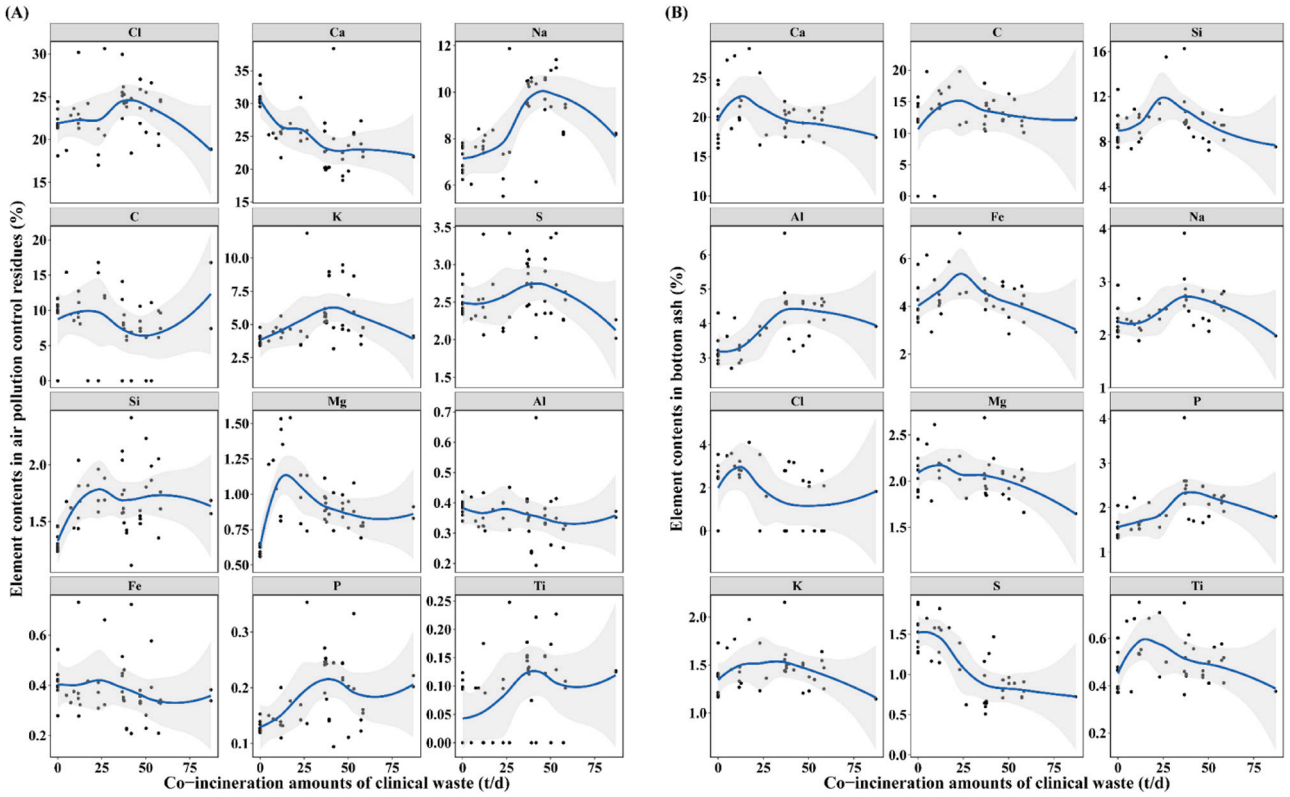

Fig. 3. Correlation between clinical waste co-incineration amounts and major element contents in the air pollution control residues (A) and bottom ash (B). The blue lines show the trend and gray zones indicate 99% confidence intervals.

emission. However, it cannot predict the effect of co-incineration on the emission of NOx, heavy metals, dioxins, etc., because their conversions are more complicated and significantly influenced by incineration conditions besides the feedstock characteristics. Owing to the possible differences in the compositions and characteristics of CW and MSW before and during the COVID-19 pandemic, the characterization of CW and MSW during the pandemic could help to increase the accuracy of the modeling result. However, sampling and analysis of COVID-19-related

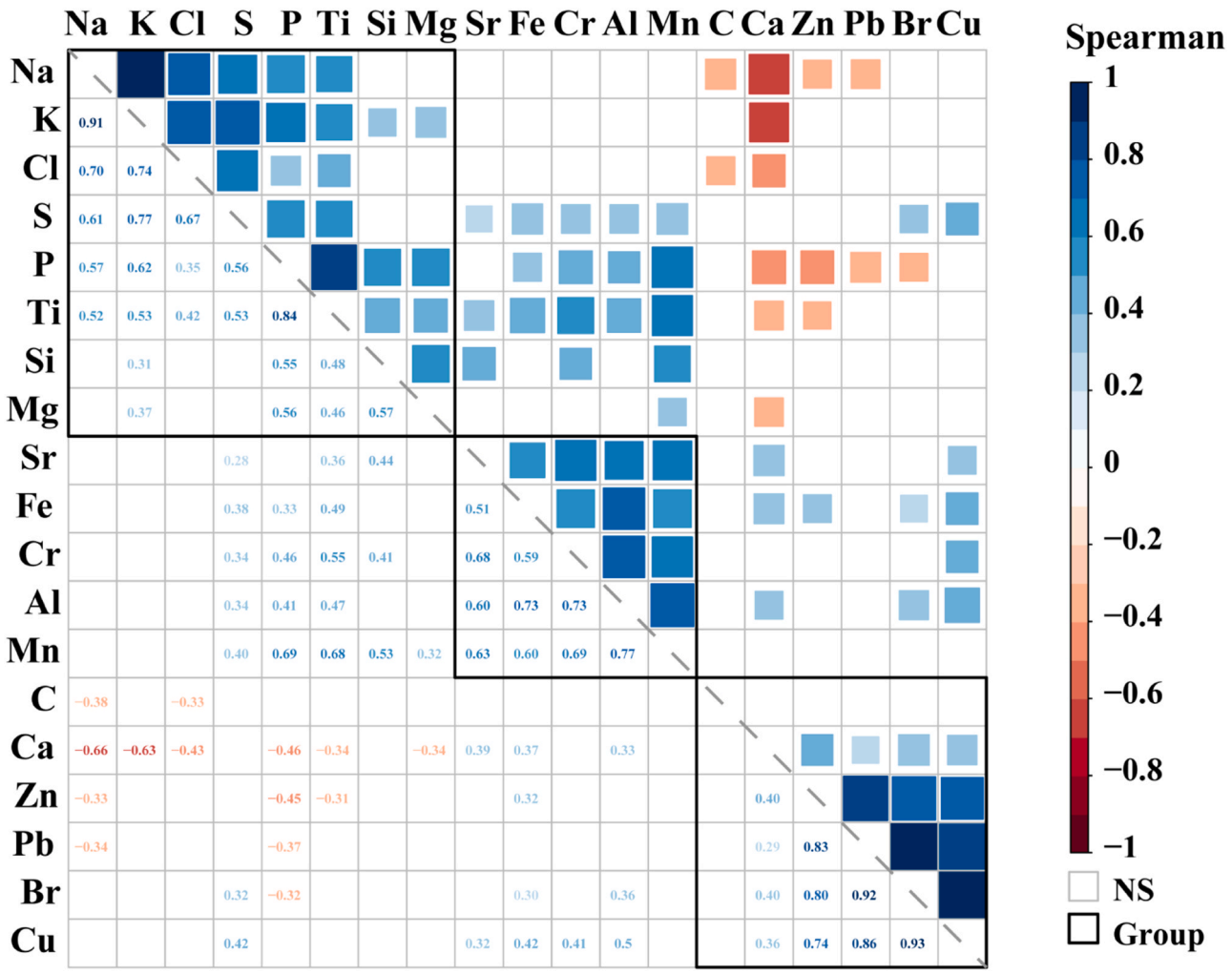

Fig. 4. Correlation matrix of element contents in the air pollution control residues. Correlation with $P > 0.05$ is considered as insignificant, and the boxes were leaved blank (NS); and rectangles around the chart (Group) are based on the results of hierarchical clustering.

CW are prohibited to prevent infection risk.

3.2. Fate of elements in the incineration residues

3.2.1. Variances in major elements

Incineration of solid waste not only emits gases (SO_2, HCl, etc.), but also generates solid residues such as APC residues and BA. To investigate the changes in major elements in the incineration residues in response to the introduction of CW in MSWI, elemental analysis of the incineration residues was conducted by using XRF. The top 6 elements were used as factors and subjected to principal component analysis (Fig. 2).

Two principal components explained 94.9% and 93.9% of the variability in the datasets of APC residues (Fig. 2A) and BA (Fig. 2B), respectively. The most common elements in APC residues were C, Ca, Cl, Na, K, and S, whereas those in BA were Ca, C, Si, Cl, Al, and Fe, which are in agreement with those reported in previous studies (Quina et al., 2008; Lindberg et al., 2015).

A good distinction in the element contents in the APC residues was observed between NCWG and CWG, which was governed by specific major contributors of the Dim2 scores, including the contents of C, Ca, Cl, Na, and K (Student's *t*-test, $P < 0.01$). On the contrary, no statistically significant difference in the element contents in BA was detected. The differences in the C and Ca contents in the APC residues can be ascribed to the variance in APC operational condition, instead of feedstock (Lindberg et al., 2015), whereas the differences in other elements in the APC residues can be attributed to the input of CW components.

Fig. 3 summarizes the contents of major elements in the APC residues (Fig. 3A) and BA (Fig. 3B) with varying CW co-incineration amounts. In the APC residues, with the increasing CW co-incineration amount from 0.0 to 87.0 t/day (<10 wt% of MSW incinerated, around 1000 t/day), the contents of Na, K, Si, P, and Ti increased; those of Ca and C decreased; and those of Cl, S, Mg, Al, and Fe showed negligible variations. Besides, the Na content (9.0% ± 1.6%) in CWG exceeded that reported in previous studies (0.6–8.4%) (Quina et al., 2008; Lindberg et al., 2015). When compared with the APC residues, the fluctuation in the major element contents in BA with varying CW co-incineration amounts was insignificant (Fig. 3B).

3.2.2. Distribution of elements

It is generally accepted that elements in waste are distributed in flue gas during MSWI by two potential processes: (i) elements are entrained by particles and (ii) elements evaporate in the furnace and exist in gas phase or condense and are adsorbed on the surface of particles (Belevi and Moench, 2000; Belevi and Langmeier, 2000; Zhang et al., 2008; Jung et al., 2004).

The results of correlation matrix and hierarchical clustering determined in the present study for the variation tendency of element richness in the APC residues (Fig. 4) are consistent with those previously reported (Jung et al., 2004). It has been indicated that Na, K, P, Ti, Si, and Mg in input waste are non-volatile and more likely to be entrained

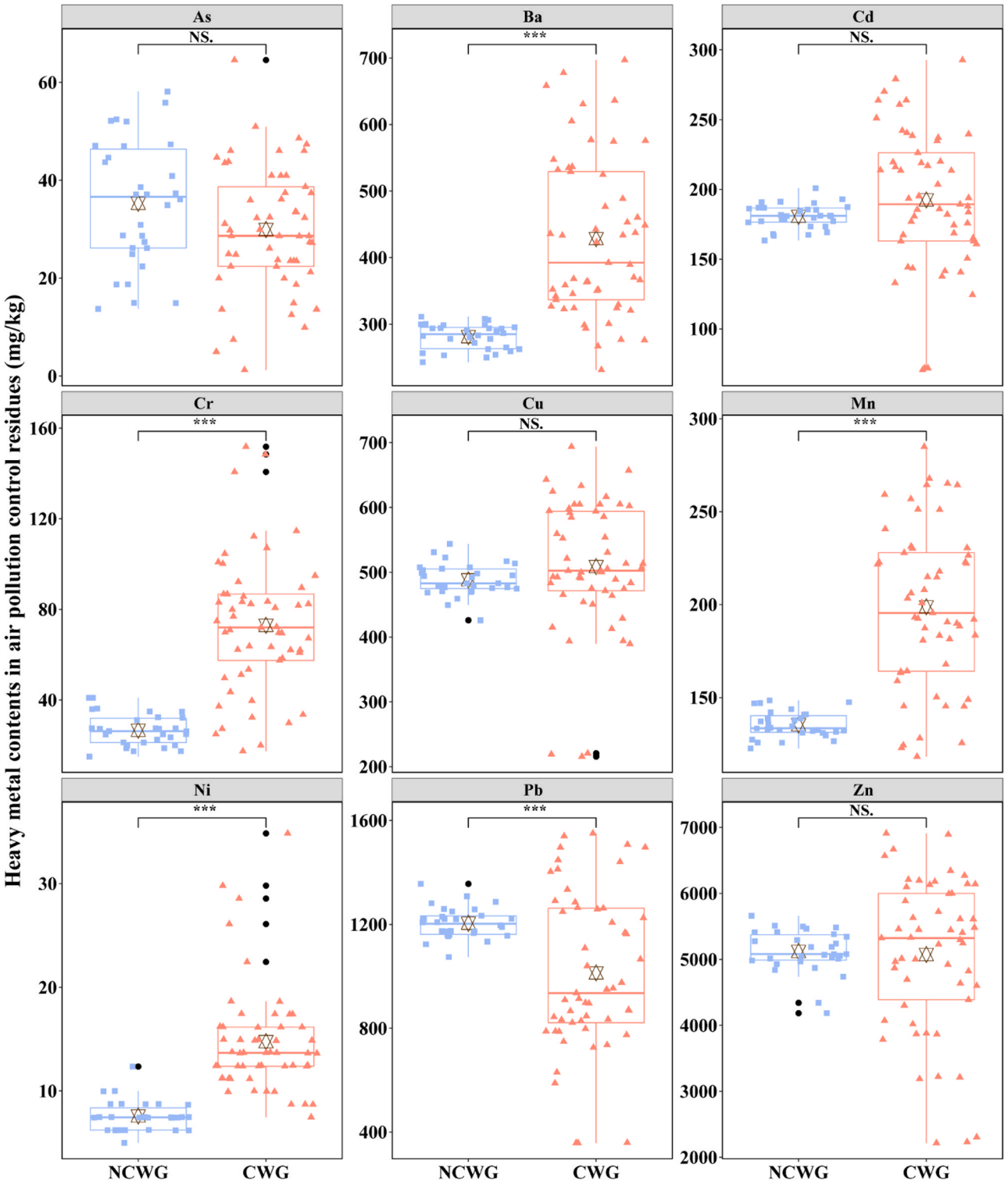

Fig. 5. Contents of heavy metals in the air pollution control residues. NCWG and CWG denote samples from incinerator without and with clinical waste input, respectively. Median, 25th, and 75th percentiles are plotted as horizontal solid lines of the boxes. The six-pointed stars represent mean values. The upper and lower whiskers extend to data no more than 1.5-times of the interquartile range from the upper and lower edge of the box, respectively. The black dots represent outliers. The results obtained using different co-incineration ratios were compared (*P* values were computed using Student's *t*-test, *** denotes $P < 0.001$, i.e., difference in the mean value is statistically significant).

into flue gas with particles and then captured into the APC residues. The elements Br, Pb, Zn, and Cu are mainly transformed by evaporation, while Mn and Cr represent the least volatile elements (Ruth, 1998).

Based on the above-mentioned data, although addition of CW in MSWI had an influence on the major constituents of the APC residues (Fig. 3A), the negligible alteration with regard to the distribution behavior of elements when the CW amounts treated in MSWI were <10 wt% was ascertained.

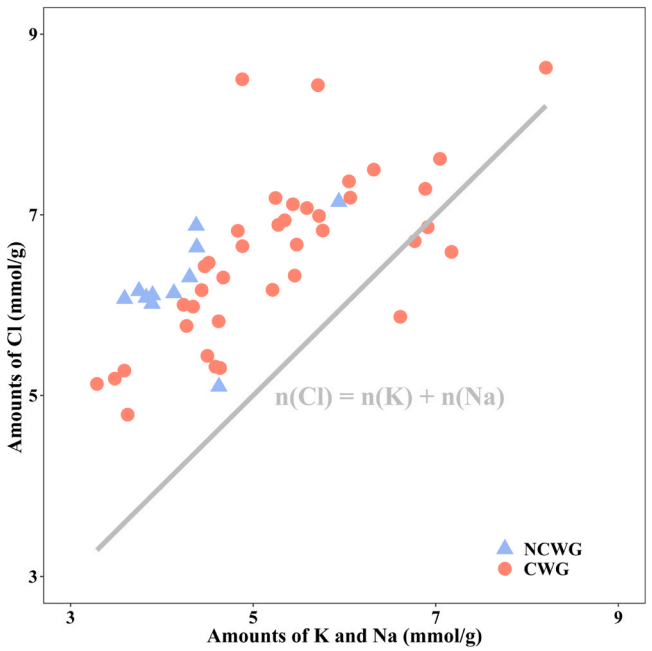

Fig. 6. Relationship between the molar amounts of Cl and sum of those of K and Na in the air pollution control residues. NCWG and CWG denote samples from incinerator without and with clinical waste input, respectively.

3.3. Adverse impact of CW co-incineration on MSWI

3.3.1. Volatilization of heavy metals

The contents of heavy metals in the APC residues analyzed by ICP-OES are shown in Fig. 5. The Ba, Cr, Mn, and Ni contents in CWG were significantly higher when CW was treated in MSWI (231–697, 17–152, 118–285, and 7–35 mg/kg, respectively), when compared with those in NCWG (243–311, 15–41, 123–149, and 5–12 mg/kg, respectively) (Fig. 5 and S2). No significant differences in the contents of As, Cd, Cu, and Zn were observed between NCWG (14–58, 163–201, 426–545, and 4185–5661 mg/kg, respectively) and CWG (1–65, 71–293, 216–694, and 2216–6909 mg/kg, respectively) (Figs. 5 and S2). The Pb content in CWG was significantly lower (358–1550 mg/kg), when compared with that in NCWG (1075 – 1356 mg/kg) (Figs. 5 and S2), and exhibited 5-fold deviation (300 mg/kg) than that in NCWG (59 mg/kg), which could be attributed to the difference in the properties of CW and MSW (Tables S1–S4). Furthermore, the contents of other heavy metals in CWG showed increased fluctuation, when compared with those in NCWG (Fig. 5).

Correlation matrix (Fig. S3) indicated that the distributions of heavy metals occurred via two processes, which was consistent with the results presented in Fig. 4. Ba, Cr, Mn, and Ni were transferred to flue gas mainly by entrainment from particulate matter (Belevi and Moench, 2000), while As, Cd, Cu, Zn, and Pb were mostly transferred via evaporation (Belevi and Langmeier, 2000). The increase in Ba, Cr, Mn, and Ni (mainly derived from alloys) contents in the APC residues of CWG could possibly be attributed to the widespread use of metallic instruments, such as needles and grippers (Kougemitrou et al., 2011), during COVID-19 pandemic.

In previous studies, the contents of Ba, Cr, Mn, and Ni in the APC residues from MSWI have been reported to be 34–14,000, 72–570, 200–1700, and 19–710 mg/kg, respectively (Lindberg et al., 2015; Jung et al., 2004); thus, the heavy metals contents in the APC residues of CWG determined in the present study are significantly lower than the upper limits described in the literature. In addition, as Ba, Cr, Mn, and Ni are difficult to leach out (Pan et al., 2013), the increase in the contents of these heavy metals had less effect on the leaching toxicity risk of the APC residues. It must be noted that CW co-incineration ratios <10 wt% had only negligible impact on BA as additives for construction materials and disposal of APC residues in security landfill.

3.3.2. Volatilization of NaCl and KCl

In general, Na and K in feedstock are released as alkali metal chlorides, and approximately 46% of Cl has been reported to be NaCl and KCl, while the rest occur as $CaCl_2$ and Friedel's salt in the APC residues sampled from the bag filter, with the injection of $Ca(OH)_2$ or CaO for acid gas removal (Zhu et al., 2008). Fig. 6 depicts the positive relationship between the molar amounts of Cl and sum of those of K and Na in the APC residues.

Owing to the strong affinity of Cl for Na and K, the relatively high contents of Cl in CW might accelerate the generation of low-melting alkali metal chlorides (NaCl and KCl) and subsequent transfer into flue gas during co-incineration (Liu et al., 2020). NaCl and KCl are prone to get deposited on the surface of the boiler, while HCl in gas phase might induce severe slagging and corrosion problems (He et al., 2020; Zhao et al., 2020). Under oxidizing conditions, HCl is oxidized at the deposit/gas interface, releasing Cl_2 (Ma et al., 2020; Ma et al., 2020). Alkali metal chlorides lower the melting temperature of deposits (Niu and Tan, 2016) and react with the protective oxide layer $(Cr, Fe)_2O_3$ to form alkali chromate and ferrate and simultaneously release Cl_2. Subsequently, the alloy materials beneath the protective oxide layer are exposed to chlorine corrosion (Israelsson et al., 2015). Therefore, co-incineration of CW in MSWI may cause boiler corrosion, further affecting the durability and service time of the boiler (Zhao et al., 2020).

4. Conclusion

This study evaluated the effects of CW co-incineration in MSWI plant during COVID-19 pandemic via simulated calculation and field sampling. A material flow model calculation was employed to assess the effects of CW co-incineration on feedstocks properties and acid gas emissions. The prediction results showed that the ash contents and LHV of CIWF as well as the concentration of HCl in flue gas were significantly increased when the CW co-incineration ratio was increased from 0 wt% to 20 wt%.

Analyses of the element contents in the APC residues and BA from MSWI with and without CW co-incineration (CWG and NCWG, respectively) revealed the following: (i) the major element contents in the APC residues significantly changed, whereas those in BA showed negligible variation in CWG, when compared with those in NCWG, and the transfer behavior of the elements in the incinerator remained similar and consisted with that reported in the literature; (ii) the contents of non-volatile heavy metals, such as Ba, Cr, Mn, and Ni, significantly increased in CWG, whereas they were still within the reported ranges in NCWG; and (iii) the increased contents of alkali metals and HCl in flue gas might exacerbate corrosion of boiler surface.

These findings provide a better understanding of the impacts of CW on MSWI and can guide future applications of co-incineration during and post pandemic.

CRediT authorship contribution statement

Dong-Ying Lan: Conceptualization, Investigation, Resources, Software, Data mining, Writing – original draft; Hua Zhang: Investigation, Resources, Methodology, Visualization, Writing – original draft, Funding acquisition, Project administration; Ting-Wei Wu: Methodology, Software, Data mining; Fan Lü:Supervision, Data curation, Formal analysis; Li-Ming Shao: Supervision, Data curation; Pin-Jing He: Writing – review & editing, Funding acquisition, Project administration, Validation.

Declaration of Competing Interest

The authors declare that they have no known competing financial

interests or personal relationships that could have appeared to influence the work reported in this paper.

Acknowledgements

We acknowledge the support from the National Key R&D Program of China (2020YFC1910100).

Appendix A. Supporting information

Supplementary data associated with this article can be found in the online version at doi:10.1016/j.jhazmat.2021.127144.

References

Bai, L.C., 2009. Incineration Treatment Engineering Technology of Municipal Solid Waste. China Building Industry Press,, Beijing.
Belevi, H., Langmeier, M., 2000. Factors determining the element behavior in municipal solid waste incinerators. 2. Lab. Exp., Environ. Sci. Technol. 34, 2507–2512.
Belevi, H., Moench, H., 2000. Factors determining the element behavior in municipal solid waste incinerators. 1. Field Stud. Environ. Sci. Technol. 34, 2501–2506.
He, X.H., Lou, C., Qiao, Y., Lim, M., 2020. In-situ measurement of temperature and alkali metal concentration in municipal solid waste incinerators using flame emission spectroscopy. Waste Manag. 102, 486–491.
Huang, Y.Y., Li, H.X., Jiang, Z.W., Yang, X.J., Chen, Q., 2018. Migration and transformation of sulfur in the municipal sewage sludge during disposal in cement kiln. Waste Manag. 77, 537–544.
Israelsson, N., Hellström, K., Svensson, J.-E., Johansson, L.-G., 2015. KCl-induced corrosion of the FeCrAl alloy Kanthal® AF at 600° C and the effect of H_2O. Oxid. Met. 83, 1–27.
Jędruchniewicz, K., Ok, Y.S., Oleszczuk, P., 2021. COVID-19 discarded disposable gloves as a source and a vector of pollutants in the environment. J. Hazard. Mater. 417, 125938.
Jung, C.H., Matsuto, T., Tanaka, N., Okada, T., 2004. Metal distribution in incineration residues of municipal solid waste (MSW) in Japan. Waste Manag. 24, 381–391.
Jung, S., Lee, S., Dou, X., Kwon, E.E., 2021. Valorization of disposable COVID-19 mask through the thermo-chemical process. Chem. Eng. J. 405, 126658.
Klemeš, J.J., Fan, Y.V., Tan, R.R., Jiang, P., 2020. Minimising the present and future plastic waste, energy and environmental footprints related to COVID-19. Renew. Sustain. Energy Rev. 127, 109883.
Komilis, D., Evangelou, A., Giannakis, G., Lymperis, C., 2012. Revisiting the elemental composition and the calorific value of the organic fraction of municipal solid wastes. Waste Manag. 32, 372–381.
Kougemitrou, I., Godelitsas, A., Tsabaris, C., Stathopoulos, V., Papandreou, A., Gamaletsos, P., Economou, G., Papadopoulos, D., 2011. Characterisation and management of ash produced in the hospital waste incinerator of Athens, Greece. J. Hazard. Mater. 187, 421–432.
Lin, X.B., Wang, F., Chi, Y., Huang, Q.X., Yan, J.H., 2015. A simple method for predicting the lower heating value of municipal solid waste in China based on wet physical composition. Waste Manag. 36, 24–32.
Lindberg, D., Molin, C., Hupa, M., 2015. Thermal treatment of solid residues from WtE units: a review. Waste Manag. 37, 82–94.
Liu, H.M., Wang, Y.C., Zhao, S.L., Hu, H.Y., Cao, C.Y., Li, A.J., Yu, Y., Yao, H., 2020. Review on the current status of the co-combustion technology of organic solid waste (OSW) and coal in China. Energy Fuels 34, 15448–15487.
Ma, S.J., Zhou, C.B., Chi, C., Liu, Yi, Yang, G., 2020. Estimating physical composition of municipal solid waste in China by applying artificial neural network method. Environ. Sci. Technol. 54, 9609–9617.
Ma, W.C., Wenga, T., Frandsen, F.J., Yan, B.B., Chen, G.Y., 2020. The fate of chlorine during MSW incineration: vaporization, transformation, deposition, corrosion and remedies. Prog. Energy Combust. Sci. 76, 100789.
F. Neuwahl, G. Cusano, J. Gómez-Benavides, S. Holbrook, S. Roudier, Best available techniques (BAT) reference document for waste incineration, Industrial Emissions Directive, European Commisssion (2010).
Niu, Y.Q., Tan, H.Z., 2016. Ash-related issues during biomass combustion: alkali-induced slagging, silicate melt-induced slagging (ash fusion), agglomeration, corrosion, ash utilization, and related countermeasures. Prog. Energy Combust. Sci. 52, 1–61.
Pan, Y., Wu, Z.M., Zhou, J.Z., Zhao, J., Ruan, X.X., Liu, J.Y., Qian, G.R., 2013. Chemical characteristics and risk assessment of typical municipal solid waste incineration (MSWI) fly ash in China. J. Hazard. Mater. 261, 269–276.
Patrício Silva, A.L., Prata, J.C., Walker, T.R., Duarte, A.C., Ouyang, W., Barcelò, D., Rocha-Santos, T., 2021. Increased plastic pollution due to COVID-19 pandemic: challenges and recommendations. Chem. Eng. J. 405, 126683.
Peng, Y.Q., Chen, J.H., Lu, S.Y., Huang, J.X., Zhang, M.M., Buekens, A., Li, X.D., Yan, J. H., 2016. Chlorophenols in municipal solid waste incineration: a review. Chem. Eng. J. 292, 398–414.
Prata, J.C., Silva, A.L.P., Walker, T.R., Duarte, A.C., Rocha-Santos, T., 2020. COVID-19 pandemic repercussions on the use and management of plastics. Environ. Sci. Technol. 54, 7760–7765.
Purnomo, C.W., Kurniawan, W., Aziz, M., 2021. Technological review on thermochemical conversion of COVID-19-related medical wastes. Resour. Conserv. Recycl. 167, 105429.
Quina, M.J., Bordado, J.C., Quinta-Ferreira, R.M., 2008. Treatment and use of air pollution control residues from MSW incineration: an overview. Waste Manag. 28, 2097–2121.
Ruth, L.A., 1998. Energy from municipal solid waste: a comparison with coal combustion technology. Prog. Energy Combust. Sci. 24, 545–564.
Shammi, M., Behal, A., Tareq, S.M., 2021. The escalating biomedical waste management to control the environmental transmission of COVID-19 pandemic: a perspective from two south asian countries. Environ. Sci. Technol. 55, 4087–4093.
Sharma, H.B., Vanapalli, K.R., Cheela, V.R.S., Ranjan, V.P., Jaglan, A.K., Dubey, B., Goel, S., Bhattacharya, J., 2020. Challenges, opportunities, and innovations for effective solid waste management during and post COVID-19 pandemic. Resour., Conserv. Recycl. 162, 105052.
Talebizadeh, M., Moridnejad, A., 2011. Uncertainty analysis for the forecast of lake level fluctuations using ensembles of ANN and ANFIS models. Expert Sys. Appl. 38, 4126–4135.
United States Environmental Protection Agency, 1996. Acid Digestion of Sludges, Solids and Soils, USEPA 3050B. Office of Solid and Hazardous Wastes, USEPA,, Cincinnati.
van Doremalen, N., Bushmaker, T., Morris, D.H., Holbrook, M.G., Gamble, A., Williamson, B.N., Tamin, A., Harcourt, J.L., Thornburg, N.J., Gerber, S.I., Lloyd-Smith, J.O., de Wit, E., Munster, V.J., 2020. Aerosol and surface stability of SARS-CoV-2 as compared with SARS-CoV-1. N. Engl. J. Med. 382, 1564–1567.
Vejerano, E.P., Holder, A.L., Marr, L.C., 2013. Emissions of polycyclic aromatic hydrocarbons, polychlorinated dibenzo-p-dioxins, and dibenzofurans from incineration of nanomaterials. Environ. Sci. Technol. 47, 4866–4874.
Wang, J., Shen, J., Ye, D., Yan, X., Zhang, Y.J., Yang, W.J., Li, X.W., Wang, J.Q., Zhang, L.B., Pan, L.J., 2020. Disinfection technology of hospital wastes and wastewater: suggestions for disinfection strategy during coronavirus Disease 2019 (COVID-19) pandemic in China. Environ. Pollut. 262, 114665.
Wang, J., Chen, Z.Q., Lang, X.J., Wang, S.L., Yang, L., Wu, X.L., Zhou, X.Q., Chen, Z.L., 2021. Quantitative evaluation of infectious health care wastes from numbers of confirmed, suspected and out-patients during COVID-19 pandemic: a case study of Wuhan. Waste Manag. 126, 323–330.
World Health Organization, 2020. WHO Coronavirus Disease (COVID-19) Dashboard. The World Health Organization, (URL:). ⟨https://covid19.who.int/⟩.
Yang, L., Yu, X., Wu, X.L., Wang, J., Yan, X.K., Jiang, S., Chen, Z.Q., 2021. Emergency response to the explosive growth of health care wastes during COVID-19 pandemic in Wuhan, China. Resour. Conserv. Recycl. 164, 105074.
You, S., Sonne, C., Ok, Y.S., 2020. COVID-19's unsustainable waste management. Science 368, 1438.
Yu, H., Sun, X., Solvang, W.D., Zhao, X., 2020. Reverse logistics network design for effective management of medical waste in epidemic outbreaks: insights from the coronavirus disease 2019 (COVID-19) outbreak in Wuhan (China). Int. J. Environ. Res. Public Health 17, 1770.
Zhang, H., He, P.J., Shao, L.M., 2008. Fate of heavy metals during municipal solid waste incineration in Shanghai. J. Hazard. Mater. 156, 365–373.
Zhang, H., Yu, S.Y., Shao, L.M., He, P.J., 2019. Estimating source strengths of HCl and SO_2 emissions in the flue gas from waste incineration. J. Environ. Sci. 75, 370–377.
Zhao, J., Li, B., Wei, X.L., Zhang, Y.F., Li, T., 2020. Slagging characteristics caused by alkali and alkaline earth metals during municipal solid waste and sewage sludge co-incineration. Energy 202, 117773.
Zhou, C.B., Yang, G., Ma, S.J., Liu, Y.J., Zhao, Z.L., 2021. The impact of the COVID-19 pandemic on waste-to-energy and waste-to-material industry in China. Renew. Sustain. Energy Rev. 139, 110693.
Zhou, P., Shi, Z.L., 2021. SARS-CoV-2 spillover events. Science 371, 120–122.
Zhu, F., Takaoka, M., Shiota, K., Oshita, K., Kitajima, Y., 2008. Chloride chemical form in various types of fly ash. Environ. Sci. Technol. 42, 3932–3937.